On Magnetic Polarity Reversal and Surface Flux Transport During Cycle 24

Xudong Sun, Todd Hoeksema, Yang Liu, Junwei Zhao; Stanford University, CA, USA (*xudong@sun.stanford.edu*)

Introduction

• Surface flux transport (SFT) model provides a phenomenological explanation to large-scale polar field reversal: redistributing active region (AR) poloidal field to global scale.

• Variations of the SFT model constituents, e.g., AR flux and tilt distribution, and meridional flow, affect cycle variation.

• We use of four-year's HMI line-of-sight magnetograms (Fig. 1) and meridional flow measurement from near-surface time-distance helioseismology to study the polarity reversal process and the variations of SFT constituents.

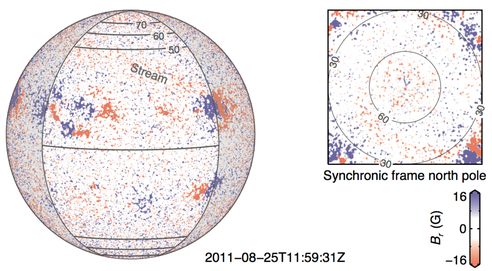

Fig 1 | Sample HMI observation. Inferred radial field magnetogram (B_r) assuming all field vectors are radial. Unshaded regions are used for mean field estimates in different latitude bands. A total of 1.6×10^5 are used. Inset shows polar field of a full Sun map (synchronic frame) for dipole calculation.

Polarity Reversal: Slow and Asymmetric

• Sunspot number (SSN) reached max in Nov 2011 for north and Feb 2014 for south (Fig. 2a), ~60% of Cycle 24.

• Polar field reversal (mean B_r above 60 deg) took place in Nov 2012 in north and Mar 2014 in south, offset by 16 months, similar to SSN (Fig. 2c).

• Axial dipole changed sign in Oct 2013; total dipole remained above 0 (Fig. 2d).

• Magnetic surges of leading-sunspot polarity N2, N4, and N5 led to multiple reversals in north; reversal in the south was delayed by surge S1 (Fig. 2b).

• Polar field reversal is very slow; recovery is slow too: weak Cycle 25?

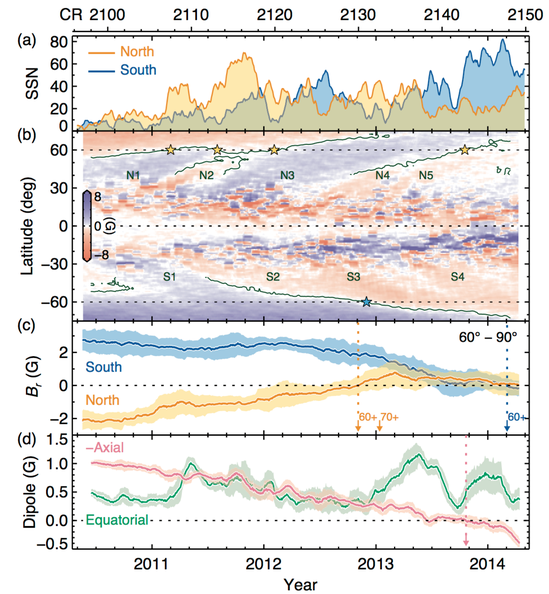

Fig 2 | Magnetic field evolution. (a) Hemispheric sunspot number (SSN). (b) Time-latitude diagram of zonally averaged B_r. Contours indicate polarity inversion; their intersection with horizontal dotted lines indicate reversals 60 degrees latitude. N1-N5 and S1-S4 mark individual surges for north and south respectively. (c) Mean field above 60 degrees as polar field. (d) Global axial and equatorial dipole computed from daily synchronic frames. Averaging window is 30 days for (a) (d); it is determined by a differential rotation profile for different latitudes for (b) (c). Vertical dotted lines and arrows mark reversal times of polar fields above denoted latitude in (c), and axial dipole in (d).

Flux Transport: Varying Meridional Flow

• CR-mean field in the surges (shaded bands in Fig. 3ad) are correlated with the AR tilt and total flux. Normal tilt and greater AR flux leads to trailing-polarity surges (Fig. 4a-d).

• Residual meridional flow demonstrates significant speed variation. Flow speed on the pole-side of activity belt is curiously dependent on the sign of the field: slower flow coincides with trailing-polarity surges (Zhao et al. 2014; Fig. 4ef).

• Surge N1 is an interesting counter-example (Fig. 4ce).

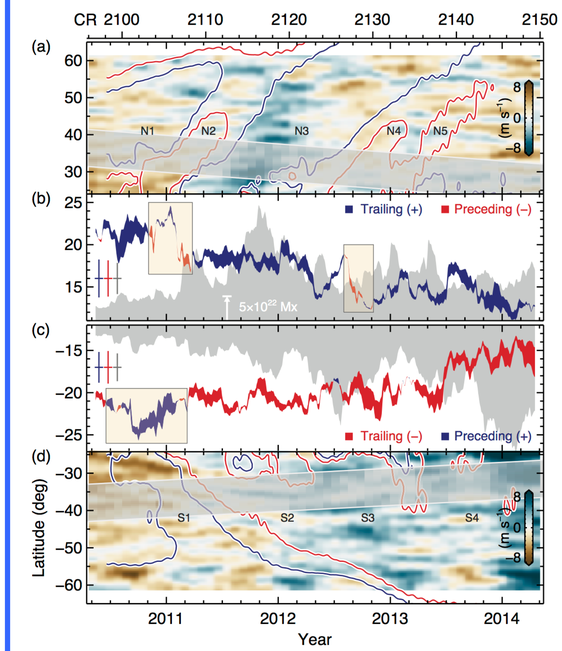

Fig 3 | Evolution of flux surges and relevant factors. (a) (d) Time-latitude diagram of zonally averaged residual meridional flow, after subtracting four-year mean.Overplotted are contours of B_r that outline the surges. Shaded bands show 10-20 degrees poleward of the mean activity belt latitude. (b) (c) Temporal profile of flux-weighted AR centroid latitude. Curve width shows the polarity separation, a proxy for the mean AR tilt angle. For north, blue (red) indicates the trailing (preceding) AR flux centroid is higher, which is equivalent to normal (inverse) tilt. For south it is the opposite. Boxes highlight periods of inverse tilt. Gray area shows the total unsigned AR flux. Only pixels below 40 degrees latitude and with B_r greater than 120 G are used for (b) (c).

Interpretation of Correlations

• **Surge field (B_r) & tilt ($\Delta\lambda$).** Preferential transequatorial cancellation of the lower-latitude component produces net flux from the higher-latitude component.

• **Surge field (B_r) & AR flux (Φ).** High Φ guarantees stable, normal tilt $\Delta\lambda$ through Joy's law, so source AR poloidal field ($P=\Phi\,\Delta\lambda$) that determines B_r (Fig. 5a) is proportional to Φ only. For low Φ, more scatter is expected in $\Delta\lambda$, thus the outlier N1.

• **Surge field (B_r) & meridional flow (δu_y).** It's linked through the Φ - δu_y relation (see blow)! Stronger positive B_r appears only during high Φ, which guarantees slower δu_y.

• **AR flux (Φ) & meridional flow (δu_y).** Helioseismology shows extended near-surface inflow around ARs (Fig. 5b). The flow is stronger for stronger AR field, providing non-linear feedback in the SFT model.

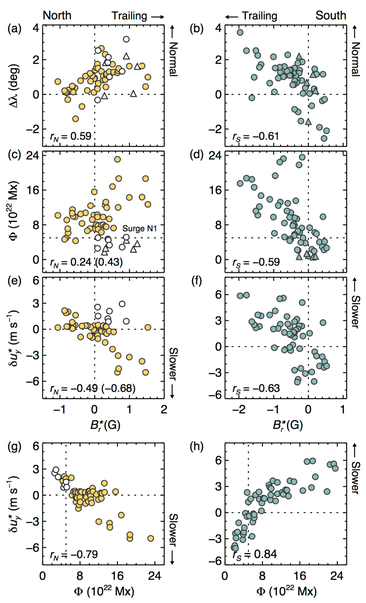

Fig 4 | Correlation between various constituents in SFT model (left). (a)-(f) Mean surge field (B_r) and mean AR tilt ($\Delta\lambda$), total unsigned AR flux (Φ), residual meridioanl flow (δu_y). (g) (h) Total flux and residual meridional flow. Left is north, right is south. Open symbols are from surge N1; triangles from MDI. Each symbol represents a CR-mean. B_r and δu_y are sampled from a band poleward of activity belt.

Fig 5 | Selective AR properties (right). (a) Sunspot butterfly diagram from DPD catalogue overplotted on time-latitude B_r diagram. Symbol size shows AR size. Color shows an AR poloidal field proxy, proportional to flux times north-south separation of two polarities. Blue symbol in north contributes to blue (positive or trailing) surges. (b) Inflow pattern around two recurring ARs.

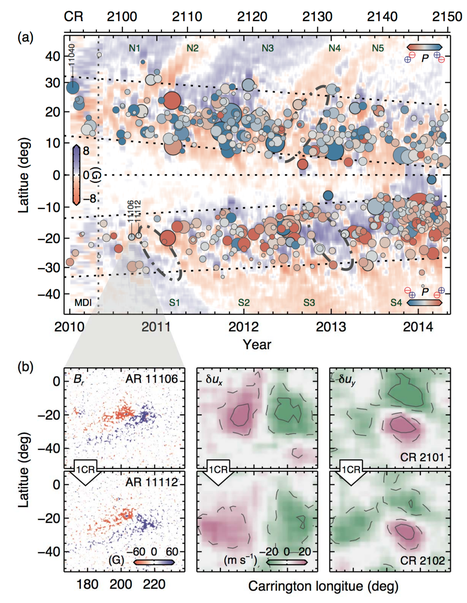

Summary & Outlook

• Cycle 24 is weak and asymmetric, consistent with predictions based on polar field of the preceding minimum, and that north-south asymmetry is common.

• New meridional flow measurement reveals interesting correlations between various constituents. All correlations and counterexamples can be explained by the SFT model, after evoking Joy's law and a field-dependent AR inflow.

• Data-driven SFT modeling with 2D meridional flow may provide new insight to cycle modulation.

➢ Sun, X., Hoeksema, J.T., Liu, Y., & Zhao, J. 2014, *ApJ*, **submitted**

➢ Zhao, J., Kosovichev, A.G., & Bogart, R.S. 2014, *ApJL*, **789**, L7

PREPRINT

goo.gl/68Ioci